Analytical Methods

Accepted Manuscript

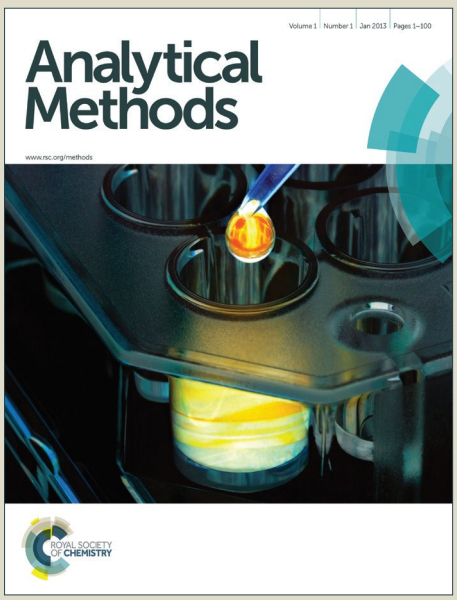

This is an *Accepted Manuscript*, which has been through the Royal Society of Chemistry peer review process and has been accepted for publication.

Accepted Manuscripts are published online shortly after acceptance, before technical editing, formatting and proof reading. Using this free service, authors can make their results available to the community, in citable form, before we publish the edited article. We will replace this *Accepted Manuscript* with the edited and formatted *Advance Article* as soon as it is available.

You can find more information about *Accepted Manuscripts* in the Information for Authors.

Please note that technical editing may introduce minor changes to the text and/or graphics, which may alter content. The journal's standard Terms & Conditions and the Ethical guidelines still apply. In no event shall the Royal Society of Chemistry be held responsible for any errors or omissions in this *Accepted Manuscript* or any consequences arising from the use of any information it contains.

ROYAL SOCIETY OF CHEMISTRY

www.rsc.org/methods

Fe_3O_4@ZrO_2 magnetic nanoparticles as a new electrode material for sensitive determination of organophosphorus agents

Na-Na Li, Tian-Fang Kang*, Jing-Jing Zhang, Li-Ping Lu, Shui-Yuan Cheng

Abstract: In this study, Fe_3O_4@ZrO_2 magnetic core-shell nanoparticles (NPs) were synthesized and were characterized by transmission electron microscopy (TEM), X-ray diffraction (XRD) and X-ray photoelectron spectroscopy (XPS). Fe_3O_4@ZrO_2 NPs were modified onto the surface of a magnetic glassy carbon electrode (MGCE) to prepare an electrochemical sensor (Fe_3O_4@ZrO_2/MGCE). The voltammetric behaviours of methyl parathion (MP) at the Fe_3O_4@ZrO_2/MGCE were studied by cyclic voltammetry. A sensitive and simple method of determination MP was developed based on the strong affinity of ZrO_2 of the sensor to phosphoric moieties of organophosphate compounds (OPs). The electrochemical sensor was successfully applied to determine MP by square-wave voltammetry (SWV). Under the optimal condition, the cathodic peak current of MP was highly linear increased with MP concentrations over the range of 7.60×10^{-8} M to 9.12×10^{-5} M, with a detection limit of 1.52×10^{-8} M.

1. Introduction

Organophosphate compounds (OPs) are primarily used as insecticides and are developed as chemical-weapon nerve agents over the world wide.[1] Therefore, developing a simple, rapid, and sensitive method for detection of low OP exposure is of great importance for human health, environmental protection.[2] Although numerous methods such as high-performance liquid chromatography (HPLC)[3] or gas chromatography coupled with mass spectrometry (GC/MS)[4] can be used to determine

Key Laboratory of Beijing on Regional Air Pollution Control, *College of Environmental and Energy Engineering, Beijing University of Technology, Beijing 100124, P. R. China*

Email: kangtf@bjut.edu.cn; kangtf@sina.cn

OPs accurately, they still suffer from some intrinsic disadvantages, e.g., complicated pretreatments of the samples, requirements of expensive instruments, well-trained operators, and inconvenience for on-site determination. Therefore, rapid, sensitive, reliable, and field deployable methods are desirable for the environment protection. Biological methods, such as ultraviolet-visible spectrophotometric method,[5] enzymatic biosensors[6, 7] and immunosensors,[8] have also been reported. Although high sensitivity can be achieved, the poor chemical or physical stability of the enzymes or antibodies prevents their use in harsh environments such as acids, organic solvents, and high temperatures. A great challenge remains to develop a rapid, reliable and sensitive method for the detection of OPs in the environments.

Electrochemical techniques offer a simple and inexpensive approach to detect OPs.[9] Nitroaromatic OPs, such as methyl parathion, paraoxon, and fenitrothion, exhibit good redox activities at different electrochemical sensors modified with advanced nanomaterials[10]. For instance, gold nanomaterials,[9] zirconia nanoparticles,[11-13] and titania nanoparticles,[14] *etc.*, are all used to construct electrochemical sensors for determining OPs. Magnetic nanomaterials have attracted much research interest during recent years because of their unique physicochemical and surface chemical properties, large surface area, and fast response under an applied external magnetic field.[15-18] However, Fe_3O_4 NPs often tend to aggregate due to their strong magnetic dipole–dipole attractions between particles as well as high specific surface area. Thus, by coated with stabilizers such as surfactants, metal nanoparticles and polymeric compounds with some specific functional groups, the Fe_3O_4 NPs are protected from oxidation and are further functionalized for stability and biocompatibility.[19,20] Magnetic nanoparticles (MNPs) can be taken to enrich target when the concentration was even low and can be conveniently separated through magnetic interaction.[21, 22] In addition, MNPs increases the electrode surface area and improve detection sensitivity.

Recent years, a number of composites of magnetic nanoparticles (NPs), *e.g.* Fe_3O_4@Au,[23] Fe_3O_4@Ag,[24] Fe_3O_4/graphene,[25] and TiO_2/SiO_2@Fe_3O_4[26], *etc.*, were reported by some authors. Zirconia, an inorganic oxide, possesses thermal stability,

chemical inertness, and nontoxic properties.[13, 27, 28] Zirconia presents a strong affinity to phosphoric moieties of OPs. There were originally some reports about the applications of zirconia in phosphopeptide enrichment, phosphoprotein capture and organophosphorus agent detection.[27, 29]

In this work, core-shell Fe_3O_4@ZrO_2 NPs were synthesized and were modified onto the surface of a magnetic glassy carbon electrode (MGCE) to prepare an electrochemical sensor (denoted as Fe_3O_4@ZrO_2NPs/MGCE). The Fe_3O_4@ZrO_2 NPs were used as an excellent matrix for trapping MP onto the electrochemical sensor (Schematic 1). To our best knowledge, there is no report about the voltammetric behavior of nitroaromatic organophosphorus pesticides at the Fe_3O_4@ZrO_2NPs modified electrodes. The research results of this work demonstrated that the electrochemical sensor can be successfully applied to determine methyl parathion by square-wave voltammetry (SWV).

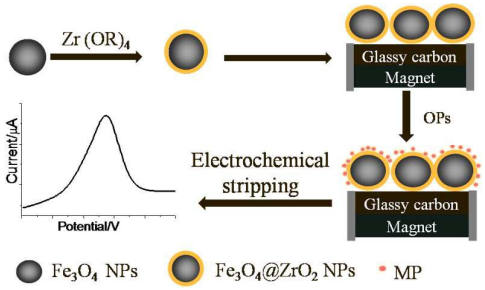

Schematic 1 Schematic illustration of the Fe_3O_4@ZrO_2 NPs as electrode material for determination of MP

2. Experimental

2.1 Apparatus and reagents

Electrochemical experiments were performed on Model CHI 842b Electrochemical Analyzer (Chen Hua Instrumental Co. Shanghai, China), in connection with a personal computer. A magnetic glassy carbon electrode (MGCE, 10 mm in diameter and 84 mm in length) with an inserted glassy carbon (3 mm in diameter and 2 mm in depth) was purchased from Tianjin Incole Union Technology Co., Ltd. (Tianjin China). A Fe_3O_4@ZrO_2 NPs modified MGCE was used as working electrode for electrochemical determination, and a platinum wire as auxiliary

electrode, a saturated calomel electrode (SCE) as reference electrode. X-ray photoelectron spectroscopy (XPS) analysis was carried out on Quantera SXM Scanning X-ray Microprobe (ULVAC-PHI INC). Transmission electron microscopy (TEM) images were obtained by HT7700 (Hitachi). Magnetization measurements of both Fe_3O_4 nanoparticles and Fe_3O_4@ZrO_2 nanoparticles were performed at room temperature using vibration sample magnetometer (VSM, Lake Shore 7410). X-ray powder diffraction (XRD) patterns of samples were collected on an X-ray diffractometer (D8 ADVANCE). Fourier transform infrared spectra (FTIR) were recorded on an IR Prestige-21 FTIR spectrometer (Shimadzu).

Methyl parathion was purchased from the Institute of Pesticide Quality Inspection Chinese Agriculture Ministry (Beijing, China). Zirconium isopropoxide was purchased from STREM Chemical Ltd. (China). $FeCl_3 \cdot 6H_2O$, $FeCl_2 \cdot 4H_2O$, and nitrophenol were obtained from Beijing Chemical Reagent Company (China). All chemicals were analytical-reagent grade materials. All solutions were prepared with ultrapure water from a Millipore milli-Q water purification system (Millipore, ≥18 MΩ cm).

2.2 Preparation of magnetic nanoparticles

Fe_3O_4NPs were synthesized using coprecipitation method.[23] In brief, 5.2 g $FeCl_3 \cdot 6H_2O$, 2.0 g $FeCl_2 \cdot 4H_2O$ and 0.85 mL of 12 M HCl were dissolved in 25 mL water that was degassed with high-pure nitrogen gas before use under stirring. Then, the mixed solution was added dropwise into 250 mL 1.5 M NaOH solution under stirring and nitrogen gas protection, followed stirring for 1 h. The obtained suspension was separated from reaction medium by magnetic field, washed, and redispersed using ultrapure water at least four times.

The Fe_3O_4@ZrO_2 NPs were prepared using sonochemical approach with a slight modification.[29, 30] In brief, 0.06 g of Fe_3O_4 NPs was dispersed into a solution obtained by dissolving 0.3 g of zirconium isopropoxide in 50 mL ethanol, and ultrasonicating for 15 min. Then a 1:5 (v/v) mixture of water and ethanol (50 mL) was added dropwise under sonication for another 2 h. After five cycles of separation/ washing/ redispersion with ethanol, the precipitate was oven-dried and calcined at 500 □ for 1

h. The furnace was then left to cool to room temperature.

2.3 Preparation of modified electrode

The MGCE was polished carefully until mirror-like with 0.05 μm alumina slurries and sequentially sonicated for 4 min in ultrapure water. The electrode was allowed to air-dry. Then 8 μL 4 mg/mL of the Fe_3O_4@ZrO_2 suspension was dropped on the surface. The Fe_3O_4@ZrO_2 NPs were firmly attached to the MGCE surface due to the magnetic force. The resulted Fe_3O_4@ZrO_2/MGCE was washed thoroughly with water and stored at 4 ℃ when not in use.

2.4 Procedure for voltammetric assay

A 20 mL aliquot of acetate buffer solution (0.08 M KCl - 0.005 M acetate of pH5.8) was placed in a voltammetric cell, and the required volumes standard MP solutions were added. The stirrer was switched on and the solution was purged with high-pure nitrogen for 10 min. Nitrogen was then passed over the solution during the experiment. The Fe_3O_4@ZrO_2/MGCE was immersed in the solution. Cyclic voltammetric detection was performed from +0.5 V to -1.1 V at a scan rate of 100 mV/s. For square wave voltammetry detection, the Fe_3O_4@ZrO_2/MGCE was immersed in the quiescent acetate buffer solution (0.08 M KCl - 0.005 M acetate of pH 5.8) containing different concentration MP under open-circuit conditions for 40s to preconcentrate the analytes. Potential scan were performed from -0.4 V to -0.9 V. The parameter settings in SWV were as following. Step potential: 4 mV; amplitude: 25 mV, and frequency: 25 Hz. All experiments were carried out at ambient temperature.

3. Results and discussion

3.1 Characterizations of magnetic nanoparticles

The sizes of Fe_3O_4 and Fe_3O_4@ZrO_2 NPs were characterized by TEM. Figure 1 (A) displays the average diameter of Fe_3O_4 NPs was about 10 nm. Figure 1(B) displays the average diameter of Fe_3O_4@ZrO_2NPs was about 20-25 nm. Figure 1 C and D show the comparison of Fe_3O_4@ZrO_2NPs suspension in the absence and presence of an external magnet. The Fe_3O_4@ZrO_2NPs suspension (Figure 1C) was homogeneous. When an external magnetic field was applied, the Fe_3O_4@ZrO_2NPs

could be separated from the solution (Figure 1D), which demonstrated that the formed magnetic Fe_3O_4@ZrO_2NPs can be firmly immobilized on the surface of MGCE by the magnetic force. [29]

Figure 2A and B show the VSM magnetization curves of Fe_3O_4NPs and Fe_3O_4@ZrO_2NPs. The Fe_3O_4NPs and Fe_3O_4@ZrO_2NPs have saturation magnetization values of 57.8 emu/g and 19.9 emu/g, respectively. These values indicated that Fe_3O_4NPs and Fe_3O_4@ZrO_2NPs were superparamagnetic and the magnetization decreased after Fe_3O_4 was coated by ZrO_2. The X-ray power diffractometer (XRD) pattern of Fe_3O_4 NPs (Figure 2C(a)) consists of six diffraction peaks at 2θ = 30.1, 35.5, 43.1, 53.4, 57.0, 62.6, which are assigned to (220), (331), (400), (422), (511), (440) reflections of Fe_3O_4, respectively.[31] In addition to pure Fe_3O_4 diffraction peaks, two new peaks at 2θ = 50.46, 60.31 were observed for Fe_3O_4@ZrO_2 (Figure 2C(b)). The positions of these new peaks match well with the (112) and (211) planes of the standard data for ZrO_2, which indicated a coating of ZrO_2 on Fe_3O_4 NPs was formed during the thermal treatment process.[28]

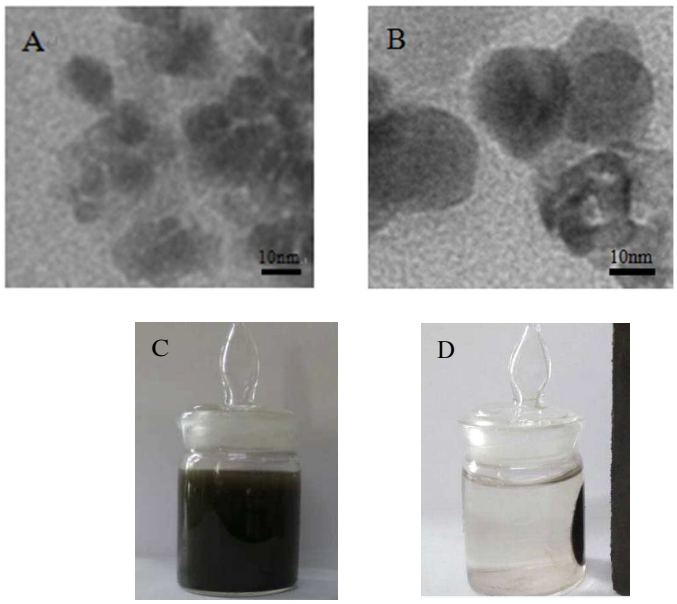

Figure 1 TEM images of (A) Fe_3O_4 NPs and (B) Fe_3O_4@ZrO_2 NPs. Photograph of Fe_3O_4@ZrO_2 NPs in the absence (C) and presence (D) of an external magnetic field.

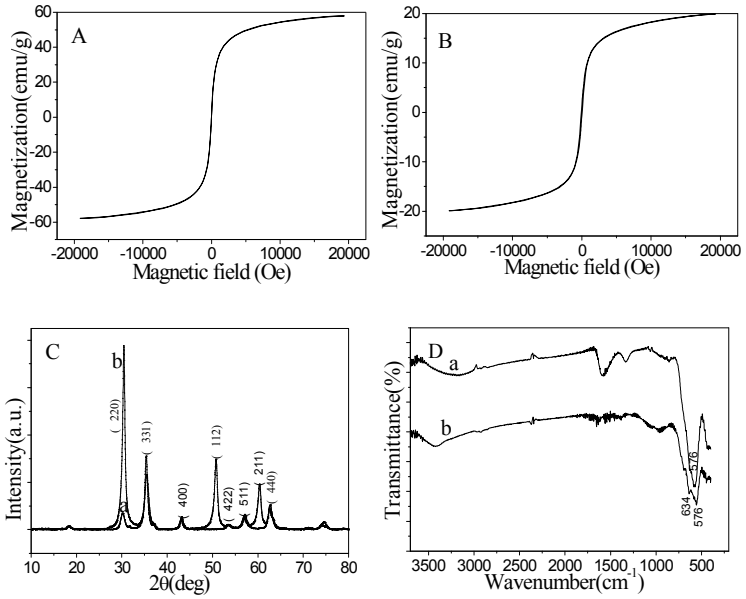

Figure 2 VSM magnetization curves of (A) Fe_3O_4 NPs and (B) Fe_3O_4@ZrO_2 NPs. (C) XRD spectra of Fe_3O_4NPs (a) and Fe_3O_4@ZrO_2NPs (b). (D) FTIR spectra of Fe_3O_4NPs (a) and Fe_3O_4@ZrO_2 NPs(b)

Figure 2D is the FTIR spectra of Fe_3O_4 NPs and Fe_3O_4@ZrO_2 NPs. The characteristic band of Fe_3O_4 NPs appears at 576 cm^{-1} (Figure 2D(a)). Compare to the Fe_3O_4NPs, a new absorption band corresponding to the characteristic absorption of zirconia at 634 $cm^{-1}$was observed (Figure 2D(b)), which furthermore confirmed the Fe_3O_4@ZrO_2 NPs were successful prepared.

XPS analysis was also performed to characterize Fe_3O_4NPs and Fe_3O_4@ZrO_2NPs (Figure 3A). Compared with the XPS spectra of Fe_3O_4 (Figure 3A(a)), two new peaks at 181.2 and 183.5 eV were observed from the XPS spectra of Fe_3O_4@ZrO_2NPs (Figure 3A(b)). In order to obtain more detailed information about the magnetic nanoparticles, the high resolution spectra of the particular regions were further investigated and these are shown in Figure 3B–D. The binding energy of 181.2 and 183.5 eV in Fig. 3B can be assigned to Zr3d5/2 and Zr3d3/2 peaks, respectively. The binding energy of 528.8 eV in Fig.3C could be attributed to the Fe–O bond. The binding energies of 723.3 eV and 709.5 eV could be assigned to Fe2p1/2, Fe2p3/2 peaks, respectively (Figure 3D).

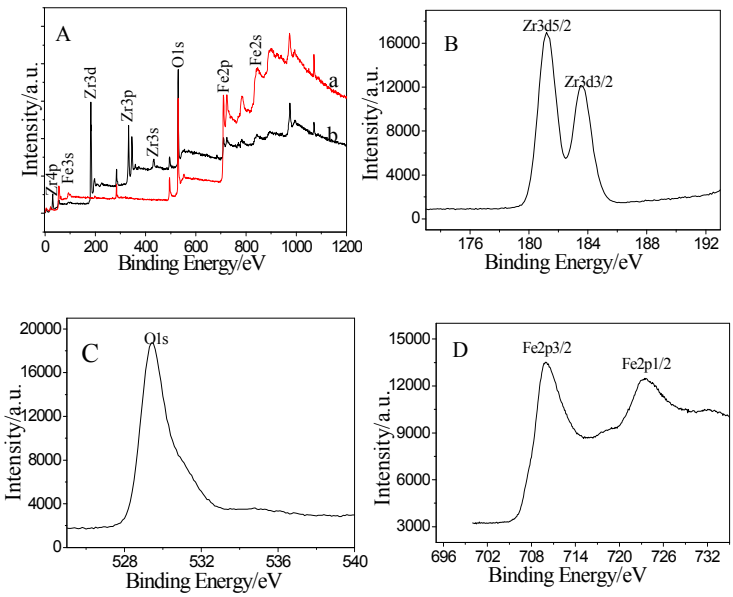

Figure 3 (A) XPS spectra of Fe_3O_4 NPs (a) and Fe_3O_4@ZrO_2 NPs(b).（B）XPS spectra of Zr3d of Fe_3O_4@ZrO_2 NPs,（C）O1s，（D）Fe2p of Fe_3O_4NPs and Fe_3O_4@ZrO_2NPs

3.2 Electrochemical behavior of methyl parathion on Fe_3O_4@ZrO_2 /MGCE

The Fe_3O_4@ZrO_2/MGCE was immersed in acetate buffer of pH 5.8 containing 5.7×10^{-5} M MP to accumulate for 40 s. Figure 4A showed the first two successive cycles of cyclic voltammograms of methyl parathion at Fe_3O_4@ZrO_2/MGCE in acetate buffer of pH5.8. A sharp irreversible reduction peak (peak 1) could be observed at -0.652 V (vs. SCE) from the cathodic scan of the first cycle. It results from the reduction of the nitro group (–NO_2) to hydroxylamine (–NHOH) via a four-electron reduction process (reaction (1))[13], which is then oxidized to the nitroso (–NO) compound during the anodic scan at −0.015 V (peak2, reaction (2)). In the successive cycles, the nitroso group is reversibly reduced to hydroxylamine with another reduction peak appeared at -0.052 (vs.SCE) (peak3, reaction (3)). The reversible redox peaks should be attributed to a two-electron redox process. These cyclic voltammograms were consistent with those described elsewhere for nitroaromatic OPs.[10]

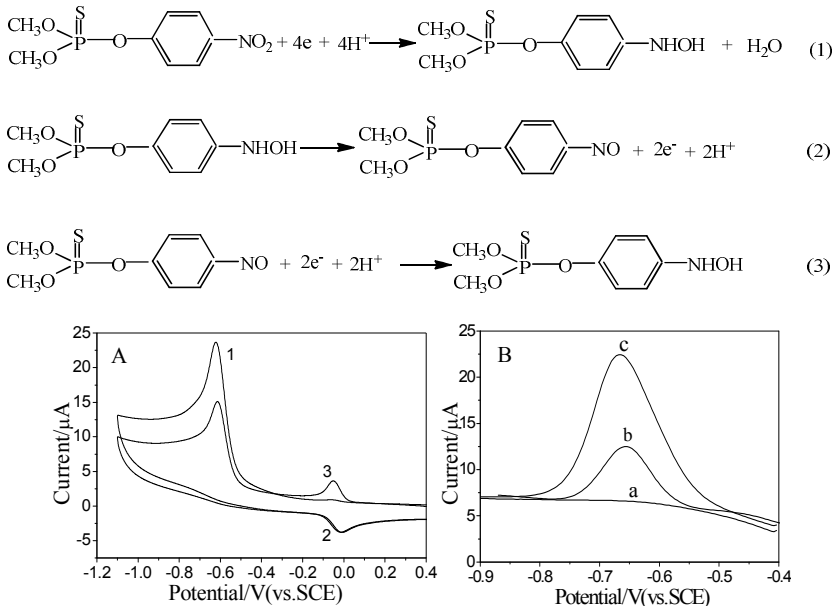

Figure 4 (A) Cyclic voltammograms of Fe_3O_4@ZrO_2/MGCE in acetate buffer containing 5.7×10^{-5} M MP to scan successive two cycles. (B) Square-wave voltammograms of Fe_3O_4@ZrO_2/MGCE in acetate buffer (a); bare MGCE (b) and Fe_3O_4@ZrO_2/MGCE (c) in acetate buffer containing 5.7×10^{-5} M MP

Compared with cyclic voltammetry, square-wave voltammetry (SWV) analysis possesses a higher sensitivity. To obtain good performance of the electrochemical response current, the irreversible reduction peak, reversible reduction peak, and oxidation peak were all examined by SWV, respectively. As shown in square-wave voltammograms (Figure 4B), no current peak was observed in acetate buffer (curve a) when Fe_3O_4@ZrO_2/MGCE was used as working electrode. After the electrode was incubated in 5.7×10^{-5} M MP for 40 s, the resulting MP/Fe_3O_4@ZrO_2/MGCE displayed a well-defined peak at 0.672 V (curve c). When bared MGCE was used as working electrode, there was a SWV peak at -0.652 V (curve b). The peak current is obviously smaller than that of MP at Fe_3O_4@ZrO_2/MGCE. Sensitive square-wave voltammetric peak can be produced by MP at Fe_3O_4@ZrO_2/MGCE (curve c). It demonstrates that the Fe_3O_4@ZrO_2NPs as a new sorbent can effectively adsorb MP because ZrO_2 possesses a strong affinity to phosphoric moieties of OPs.[10, 27]

3.3 Optimization of the analytical conditions

Figure 5A shows the effects of the amount of Fe_3O_4@ZrO_2NPs on the SWV peak current of MP at the Fe_3O_4@ZrO_2 /MGCE. Fe_3O_4@ZrO_2NPs aqueous suspension of 4 μg/μL was adopted throughout the study. One can see that the stripping peak currents increased with increasing the amount of Fe_3O_4@ZrO_2 NPs up to 8 μL, i.e. 32 μg Fe_3O_4@ZrO_2 NPs. But the amount of Fe_3O_4@ZrO_2 is more than 8 μL, the cathodic peak current decreases with the gradual increase of the Fe_3O_4@ZrO_2. The decrease of the current can be understood by considering the Fe_3O_4@ZrO_2 layer thickness which caused higher resistance for the electrochemical processes, hindering the electronic exchange between the methyl parathion and the Fe_3O_4@ZrO_2/MGCE, leading to a decrease of the sensitivity of current response (Figure 5A). Therefore, 32 μg Fe_3O_4@ZrO_2 was selected for the optimal magnetic nanoparticles amount to modified each MGCE electrode.

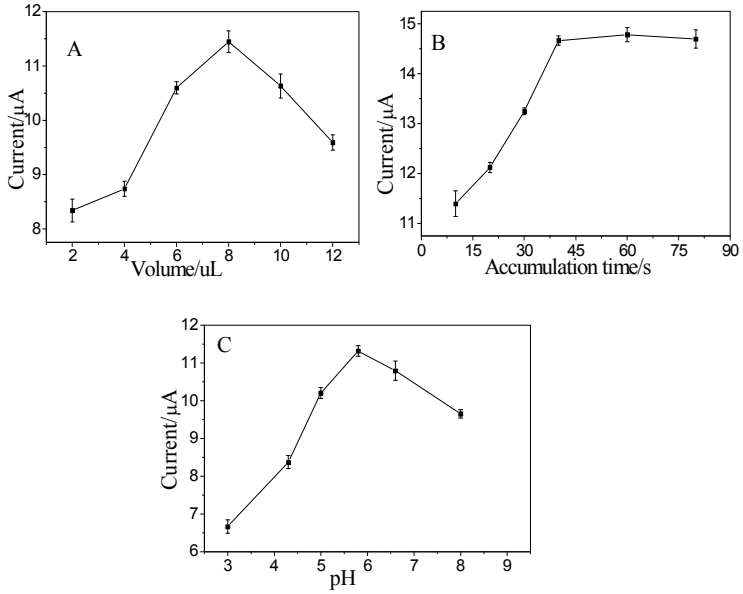

Figure 5 (A) Effects of Fe_3O_4@ZrO_2 amount, (B) accumulation time, and (C) pH of buffer solution on the SWV peak current of MP at the Fe_3O_4@ZrO_2 /MGCE. The enrichment experiments were performed in acetate buffer containing 3.8×10^{-5} M MP. SWV determination conditions as in Fig.4

The effect of accumulation time on the response of Fe_3O_4@ZrO_2/GCE was investigated with 5.7×10^{-5} M MP (Figure 5B). The peak current increases rapidly with

the accumulation time up to 40 s. With longer accumulation times, the peak current with accumulation time did not increased. The adsorption of methyl parathion on the Fe_3O_4@ZrO_2 /MGCE becoming more and more saturated. The resulting current versus time plot displays a curvature consistent with adsorption processes. We also observed the adsorption of methyl parathion under potentiostatic conditions (not shown), the experimental results indicated that the reduction peak current of methyl parathion did not significant increase. The rapid and effective enrichment of MP is due to the strong affinity between ZrO_2 and OPs. Thus, the accumulation time of 40s was chosen. In this study, the accumulation time is shorter than those reported in literaturesthat MP was determined by SWV, e.g. 5 min[12] or 2 min[13] of accumulation time was adopted, when a ZrO_2 NPs modified carbon paste electrode[12] or a ZrO_2 NPs modified glassy carbon electrode[13] was used, respectively.

The pH is an important parameter that affects the adsorption of MP on the electrode surface. In this study, the effect was investigated over a pH range from 3.0 to 8.0. Figure 5C presents the effect of the solution pH on the SWV cathodic peak current of 3.8×10^{-5} M MP. It can be seen that the peak current increases with an increase of pH up to 5.8, and then it decreases at higher pH (5.8–8.0). It indicates that Fe_3O_4@ZrO_2 nanoparticles have the maximum adsorption to methyl parathion in a weakly acid environment. Although the lower pH value is favourable to electroreduction according to the mechanism of showed above by reactions (1)–(3), the substantial reduction current of hydrogen ions in lower pH range such as 4.0 will interfere with the determination of MP. Therefore, pH 5.8 of 0.08 M KCl - 0.005 M acetate buffer solutions was used as the supporting electrolyte solutions in the experiments.

3.4 Analytical performance

Figure 6 displays the SWV response of the Fe_3O_4@ZrO_2/GCE to different concentration MP. Well-defined peaks, proportional to the concentration of the corresponding MP, were observed. The reduction peak current (i_p) was linearly increased with the increase of MP concentration (c) over the concentration range from 7.60×10^{-8} to 9.12×10^{-5} M. The linear regression equations is i_p(μA) = 0.300 c (μM) +

0.774, with a correlation coefficient of 0.9998 and a detection limit of 1.52×10^{-8} M, which was calculated from the signal-to-noise ratio of 3.

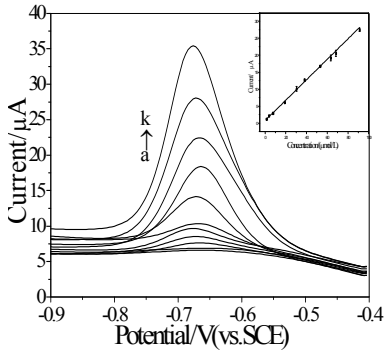

Figure 6 Square-wave voltammograms of MP

From bottom to top, the concentration of MP was (a) 0, (b) 7.60×10^{-8}, (c) 1.52×10^{-6} , (d) 3.04×10^{-6}, (e) 4.56×10^{-6}, (f) 7.60×10^{-6}, (g) 1.90×10^{-5}, (h) 3.80×10^{-5}, (i) 5.70×10^{-5}, (j) 7.60×10^{-5} and (k) 9.12×10^{-5} M. The inset shows the calibration curve. SWV determination conditions as in Fig.4

The performances of the sensor proposed by this paper were compared with those of sensors previously described. The proposed sensor possesses a series of advantages, for example, more simple fabrication procedure than those of sensors which involved in the electrodeposition of metal nanoparticles[9,32] and a lower detection limit than those obtained with gold nanoparticle/Nafion[32], gold nanoparticle/sodium dodecylbenzene[9], or silver nanoparticles/Nafion[2] modified GCE. Table 1 lists the comparison for the determination of MP by different sensors.

Table1 Comparison of proposed sensor for determination of MP with others.

Electrode	Modifier	Methods	Detection limit (μg/L)	Refs.
GCE	gold nanoparticles/Nafion	SWV	26.3	[32]
GCE	gold-sodium dodecylbenzene	SWV	22.6	[9]
GCE	nanosilver/Nafion	DPV	74.1	[2]
MGCE	Fe_3O_4@ZrO_2	SWV	4.0	present

3.5 Reproducibility and interferences

The reproducibility of the Fe_3O_4@ZrO_2/MGCE was investigated in the presence of 7.2×10^{-5} M MP in acetate buffer solution. SWV experiments were repeatedly performed for 6 times with the same Fe_3O_4@ZrO_2/MGCE in the acetate buffer containing 7.2×10^{-5} M MP. The relative standard deviation was 5.2 %. Similarly, the fabrication reproducibility of the sensor was investigated by SWV experiment using eight different electrodes respectively in acetate buffer containing 7.2×10^{-5} M MP. The relative standard deviation (RSD) of the peak current values of the eight electrodes was 3.4%, indicating acceptable fabrication reproducibility. To achieve the regeneration of the sensor, the multiple successive cyclic voltammetric scanning was used to remove the MP until the stripping peak disappeared completely.

In order to assess the selectivity of the electrochemical sensor, interference studies were carried out with inorganic or organic species. No interference could be observed for the following materials: Mg^{2+} (100), Fe^{3+} (100), CO_3^{2-} (100), NO_3^- (100), dimethoate (10), carbofuran (10), nitrophenol (5), where the data in brackets denote the molar ratio of the interfering compound to 5.7×10^{-5} M MP. (Fig.7).

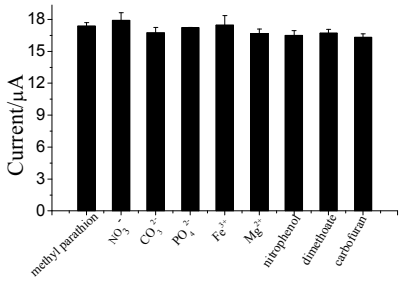

Figure 7 The effects of interference of different species on the SWV peak current of MP.

3.6 Analytical applications

The sensor was used to the determination of MP in vegetable samples by the standard addition method.[32] Vegetable samples (lettuce, cabbage) were obtained from the local markets and cleaned by tap water and ultrapure water in turn. An amount of 5.00 g of each sample was spiked with 10.0 mg/mL MP. After 12 h, the samples were

extracted with 30 mL ether. The supernatants were taken and filtered through a 0.45 μm membrane and then evaporated to dryness.[10] A 2 mL ethanol was added to the dry residue and diluted to 100mL with acetate buffer solution. Table 2 summarizes the determination results of the sensor. As can be seen from Tables 2, the recoveries are acceptable for all the samples.

Table 2 Determination of MP in vegetable sample (n=4)

Samples	Added (10^{-5}/(M))	Found (10^{-5}/(M))	Mean recovery(%) ±S.D.(n=4)
Lettuce	3.8	3.95	103.9±0.07
Cabbage	3.8	3.73	98.2±0.26

4. Conclusions

In this study, a sensitive electrochemical sensor was developed for the rapid determination of methyl parathion based on Fe_3O_4@ZrO_2NPs. With the unique characteristic of zirconia, the sensor exhibited strong adsorption and stripping for methyl parathion. Based on the Fe_3O_4@ZrO_2/MGCE electrochemical sensor, methyl parathion was determined with wide linear ranges, low detection limit, and acceptable reproducibility. The electrochemical sensor shows great potential for the sensitive and fast detection of methyl parathion.

Acknowledgements

This work was supported by the Doctoral Foundation of China Education Ministry (No. 20131103110011), and the Key Project of Beijing Natural Science Foundation (No. KZ201110005006).

References

1 J. H. Lee, J. Y. Park, K. Min, H. J. Cha, S. S. Choi and Y. J. Yoo, *Biosens. Bioelectron.*, 2010, **25**, 1566-1570.

2 A. Kumaravel and M. Chandrasekaran, *J. Electroanal. Chem.*, 2010, **638**, 231-235.

3 Z. Xu, G. Fang and S. Wang, *Food Chem.*, 2010, **119**, 845–850.

4 A. R. Fontana, A. B. Camargo and J. C. Altamirano, *J. Chromatogr. A*, 2010, **1217**, 6334–6341.

5 Z. Li, Y. Wang, Y. Ni and S. Kokot, *Sens. Actuators, B*, 2014, **193**, 205-211.

6 F. Arduini, S. Guidone, A. Amine, G. Palleschi and D. Moscone, *Sens. Actuators, B*, 2013, **179**, 201-208.

7 X. Meng, J. Wei, X. Ren , J. Ren and F. Tang, *Biosens. Bioelectron.*, 2013, **47**, 402-407.

8 X. Zhang, H. Wang, C. Yang, D. Du and Y. Lin, *Biosens. Bioelectron.*, 2013, **41**, 669-674.

9 C. Li, Z. Wang and G. Zhan, *Colloids Surf., B*, 2011, **82**, 40-45.

10 R. Xue, T. F. Kang, L. P. Lu and S. Y. Chen, *Anal. Lett.*, 2013, **46**, 131-141.

11 J. Gong, X. Miao, H. Wan and D. Song, *Sens. Actuators, B*, 2012, **162**, 341 -347.

12 H. Parham and N. Rahbar, *J. Hazard. Mater.*, 2010, **177**, 1077-1084.

13 G. Liu and Y. Lin, *Anal. Chem.*, 2005, **77**, 5894-5901.

14 A. Kumaravel and M. Chandrasekaran, *J. Electroanal.Chem.*, 2011, **650**, 163-170.

15 A. Nomura，S. Shin，O. O. Mehdi and J. M. Kauffmann, *Anal. Chem.*, 2004, **76**, 5498-5502.

16 D. Yu，B. Blankert，E. Bodoki，S. Bollo, J. C. Vire, R. Sandulescu, A. Nomura, and J. M. Kauffmann , *Sens. Actuators, B*，2006, **113**, 749-754.

17 G. Bayramoglu and M. Y. Arica, *J. Hazard. Mater.*, 2008, **156**, 148-155.

18 L. M. Rossi, A. D. Quach and Z. Rosenzweig, *Anal. Bioanal. Chem.*, 2004, **380**, 606-613.

19 E. E. Carpenter, *J. Magn. Magn. Mater.*, 2001, **225**, 17-20.

20 Y. Liu, W. Zhu, D. Wu and Q. Wei, *Measurement*, 2015, **60**, 1-5.

21 S. Nourani, H. Ghourchian, S. M. Boutorabi, *Anal. Biochem.*, 2013, **441**, 1-7.

22 X. Zhao, Y. Shi, Y. Cai, and S. Mou, *Environ. Sci. Technol.,* 2008, **42***,* 1201–1206.

23 W. Liu, Y. Zhang, S. Ge, X. Song, J. Huang, M. Yan and J. Yu, *Anal. Chim. Acta*, 2013, **770**, 132-139.

24 E. Tahmasebi and Y. Yamini, *Anal. Chim. Acta*, 2012,**756**, 13-22.

25 Y. P. Chang, C. L. Ren, J. C. Qu and X. G. Chen, *Appl. Surf. Sci.*，2012, **261**, 504 -509.

26 H. Liu , Z. Jia, S. Ji, Y. Zheng, M. Li and H. Yang, *Catal. Today*, 2011, **175**,

293-298.

27 D. Du, J. Liu, X. Zhang, X. Cui and Y. Lin, *J. Mater. Chem.*, 2011, **21**, 8032-8037.

28 A. P. Kumar, J. H. Kim, T. D. Thanh and Y. I. Lee, *J. Mater. Chem. B*, 2013, **1**, 4909-4915.

29 H. P. Peng, R. P. Liang, L. Zhang and J. D. Qiu, *Electrochim. Acta.*, 2011, **56**, 4231- 4236.

30 Y. Li, T. Leng, H. Lin, C. Deng, X. Xu, N. Yao, P. Yang and X. Zhang, *J. Proteome Res*., 2007, **6**, 4498-4510.

31 Y. R. Cui, C. Hong, Y. L. Zhou, Y. Li, X. M. Gao and X. X. Zhang, *Talanta*，2011, **85**, 1246-1252.

32 T. F. Kang, F. Wang, L. P. Lu, Y. Zhang and T. S. Liu, *Sens. Actuators, B*, 2010, **145**, 104-109.